JOURNAL OF SPACECRAFT AND ROCKETS
Vol. 36, No. 2, March–April 1999

Aerothermodynamic Overview, X-34

Henri D. Fuhrmann,* John Hildebrand,† and Tony Lalicata‡
Orbital Sciences Corporation, Dulles, Virginia 20166

THE purpose of this paper is to provide an overview of the X-34 technology program and to serve as an introduction to the papers that follow in this special section. Orbital Sciences Corporation (OSC) is developing a reusable launch vehicle (RLV) technology demonstrator called the X-34 for NASA's RLV program.[1] This low-cost, liquid-fueled, rocket plane is designed to demonstrate new operational approaches and technologies that will dramatically reduce the time and cost required to process and operate future launch vehicles. The overall goal of NASA's RLV program is to demonstrate the key technologies needed to lower dramatically the cost of putting a pound of payload into space by a factor of 10 or more.

The X-34 is a winged, hypersonic vehicle that will be air launched from the belly of OSC's L-1011 carrier aircraft. It will be capable of reaching speeds of up to Mach 8 at altitudes up to 250,000 ft. OSC relies heavily on experience with their air-launched Pegasus and ground-launched Taurus systems. In fact, the X-34 ascent trajectory and performance targets are very similar to those of the Pegasus first stage. In this way X-34 is demonstrating advanced technologies, low-cost operations, and rapid processing of a first-stage launch vehicle from which comparisons with expendables can be made.

The X-34 will also be used to demonstrate autonomous flight, all-graphite/epoxy composite construction, a composite propellant tank, flexible thermal protection blankets, and new silicone-impregnated leading-edge tiles. The operating goals of the X-34 are a two-week turnaround between launches and a one-time, 24-h turnaround. The X-34 may also be called upon to demonstrate autonomous landings in cross winds of up to 20 kn. Each of the operating goals set by NASA is intended to simulate aircraft-like operations of a launch vehicle.

Whereas previous "X" programs have pushed the edge of the performance envelope, the X-34 program seeks to build on the experience garnered from vehicles such as the X-15 by matching or slightly exceeding performance with an order-of-magnitude reduction in development and operations costs. In this way, the X-34 is attempting to break the barrier of high cost and burdensome operations that limits affordable access to space.

A typical X-34 flight profile (Fig. 1) consists of a drop from the L-1011 aircraft at an altitude of approximately 38,000 ft and Mach 0.75, engine ignition and acceleration to the planned Mach number and altitude, a coast phase, re-entry, and landing. The elevons, rudder, body flap, and speed brake provide control and trim during powered and unpowered flight, aided by reaction control during the high-altitude coast phase. Thrust vector serves as the primary pitch and yaw trim controller during flight under main engine propulsion.

The X-34 program relies heavily on analysis and equipment furnished by many of the NASA centers, as well as other government agencies. The Fastrac engine used to power the X-34 is being developed by NASA Marshall Space Flight Center (MSFC), the silicone impregnated reusable ceramic ablator (SIRCA) leading-edge tiles are designed and built by NASA Ames Research Center, the NASA Dryden Flight Research Center supports ground vibration and captive carry testing, the Kennedy Space Center will be the site for envelope expansion flights, and the NASA Langley Research Center is responsible for the aerodynamic heating and flight characteristics of the X-34.

Aggressive cost and schedule requirements dictated a concurrent engineering approach in which the design and analysis of the vehicle were conducted in parallel with fabrication and testing. The X-34 outer mold line (OML) was frozen only two months after NASA and OSC signed the contract to build and fly the X-34. Five months later, the aerodynamic heating analysis was completed. This very fast pace required compromise and an appropriate balance of schedule and technical risk.

This paper serves as an overview of the analyses and tests conducted by the NASA Langley Research Center, NASA Ames Research Center, Oceaneering Thermal Systems (OTS), and OSC aerothermal team and presented in this X-34 Special Section. The process of determining thermal requirements and analyses to support the selection and validation of the X-34 thermal protection system (TPS) is covered.

X-34 Design

Cost and schedule, as well as performance requirements, drove the design of the X-34. They required that the aerodynamic design of the current X-34 vehicle draw heavily from the X-34B program,[2] which in turn extensively utilized data and design experience generated from the Space Shuttle program. As a result, the X-34 double delta wing planform has an 80–45-deg leading-edge sweep angle and elevon area ratios similar to those of the Shuttle Orbiter (Fig. 2).

Most of the vehicle is covered with thermal protection blankets. They consist of three types of blanket, each with varying temperature and insulation capability: 1) high heat blanket (HHB) with 2000°F multiuse capability [similar to the Advanced Flexible Reusable Surface Insulation (AFRSI) used on the Shuttle Orbiter but with upgraded materials for high temperature and insulation capability]; 2) low heat blanket (LHB) with 1500°F multiuse capability [similar to the HHB but with reduced material properties that result in both lower cost and temperature capability]; and 3) Felt Reusable Surface Insulation (FRSI) blanket with 700°F multiuse capability (identical to that used on certain areas of the Shuttle Orbiter where fairly benign heating conditions are reached). The nose cap, wing leading edge, and rudder leading edge are made up of SIRCA tiles.

Several competing factors led to the final airfoil shape, which is quite different from that of the Shuttle Orbiter. Design constraints were that the airfoil have a flat bottom for ease of manufacturing and blending with the fuselage, that the outboard wing section have a constant leading-edge radius for a common leading-edge tile design, and that sufficient internal volume be provided for packaging the main landing gear and actuator devices. The result is a flat-bottomed airfoil with high upper surface camber and varying spanwise thickness-to-chord ratio from 9.2% at the sweep break point to 13.4% at the wing tip.

In addition to the manufacturing requirements, the leeward-side thermal protection blankets vary in thickness chordwise as insulation requirements are more severe toward the leading edge. These compromises produce a wing with a sufficient low-speed lift-to-drag ratio and adequate supersonic and hypersonic handling characteristics[3] while meeting structural and thermal design and manufacturing goals.

The X-34 is powered by the 60,000-lbf-thrust Fastrac engine, which uses liquid oxygen (LOX) and kerosene (RP).[4] Under powered conditions the engine nozzle gimbals to provide pitch and yaw trim. Elevon, body flap, and speed brake control surfaces are also used for pitch control during both the powered and unpowered phases of flight (Fig. 3). The all-moving vertical tail and asymmetric elevon deflections provide lateral/directional control.

The X-34 system design requires that the TPS insulate to within 50°F of the 350°F temperature limit of the structure.[5] Therefore, thermal analyses were required to show that the structure never exceeds 300°F. The 50°F margin is used to account for trajectory

*X-34 Aerodynamics Lead. Member AIAA.
†X-34 Thermal Lead. Member AIAA.
‡X-34 Senior Thermal Analyst. Member AIAA.

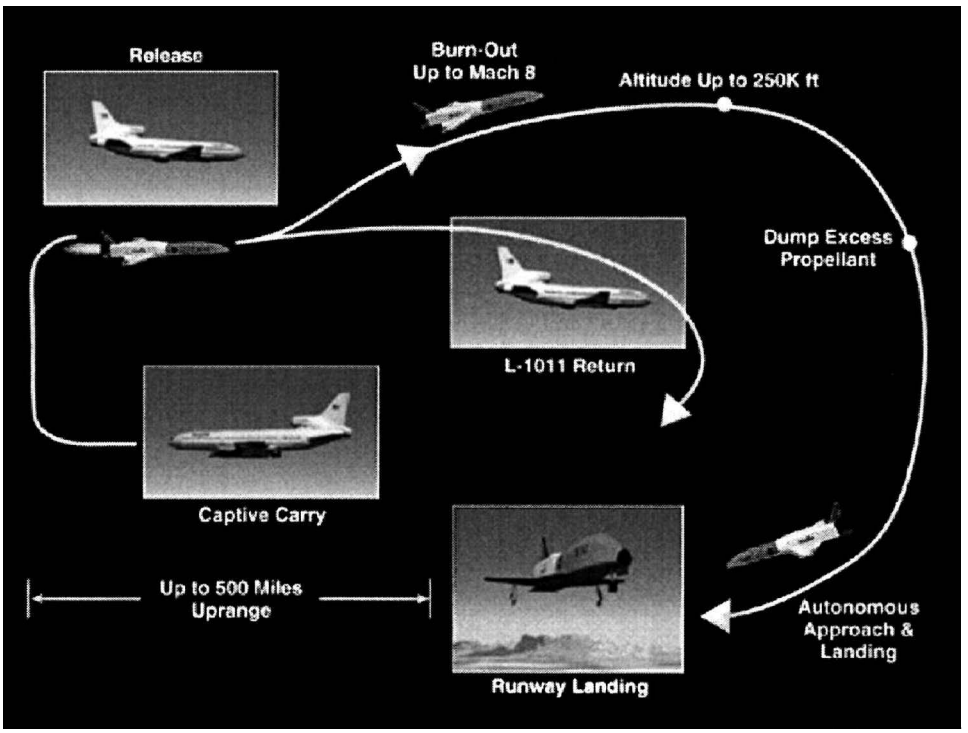

Fig. 1 X-34 flight profile.

Reference Numbers	
Sref	357.5 ft^2
mac	174.48 in.
bref	332 in.
mrc	420 in. wrt the nose

X-34 Geometry	Component	
	Wing	All-Moving Vertical Tail
Area	357.5 ft^2	33.0 ft^2
Span	332.9 in.	75.5 in.
Aspect Ratio	2.14	1.2
Taper Ratio		
Sweep (LE)	45°	40°
Dihedral	6°	–
Incidence	0	–
MAC	174.5 in.	64.5 in.
Control	**Area**	**Maximum Deflection**
Inboard Elevon	14.5 ft^2	-34.2 to +15.8°
Outboard Elevon	14.9 ft^2	-34.2 to +15.8°
All-Moving Vertical Tail	33.0 ft^2	+/- 30°
Speedbrake	11.0 ft^2	-13.6° to 90°
Body Flap	22.3 ft^2	-10 to 20°

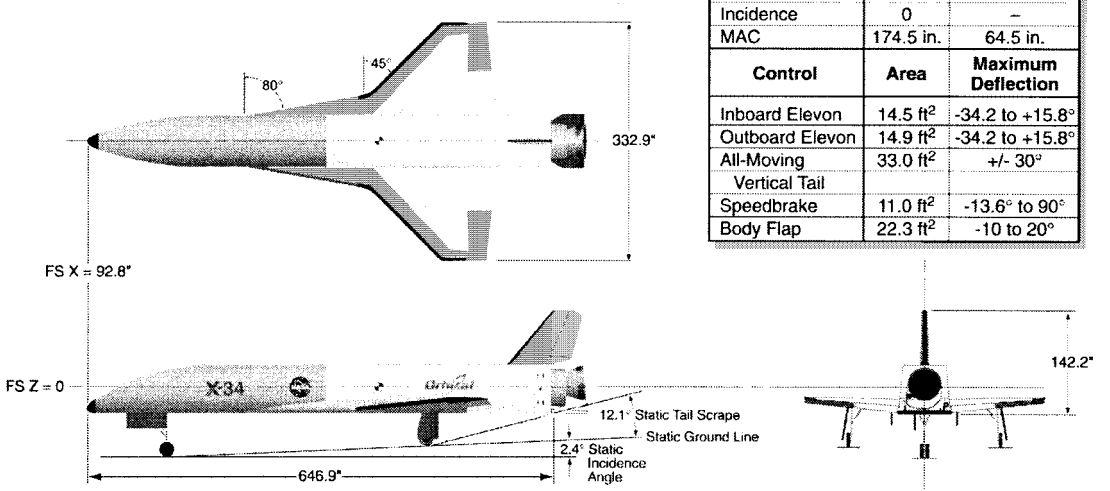

Fig. 2 X-34 geometry.

dispersions, TPS fabrication anomalies, and uncertainties in heat transfer and soak-back rates.

OML requirements and cost constraints dictated that the windward surface of the vehicle be protected with constant-thickness TPS blankets for which $\frac{3}{4}$-in. HHB was selected. Because the blanket with highest temperature and insulation properties was chosen, very high thermal protection margins for most of the windward side of the vehicle result. More design flexibility for blanket type and thickness selection was afforded on the leeward side of the vehicle. For this reason, most of the detailed aerodynamic heating analysis conducted by NASA Langley Research Center was focused on obtaining maximum leeward heating environments. The results are leeward blanket distributions and types that minimize weight and cost while meeting the thermal protection requirements.

Typical X-34 Mission

The X-34 is capable of flights from unpowered approach and landing tests to full-burn, maximum-Mach-number trajectories. NASA has undertaken an envelope expansion approach in which performance limits will be reached incrementally throughout the 27-flight program. This means that unpowered tests will precede powered flights to low supersonic Mach numbers, which in turn will precede maximum Mach and heating condition flights. The envelope expansion approach allows for validation and correlation

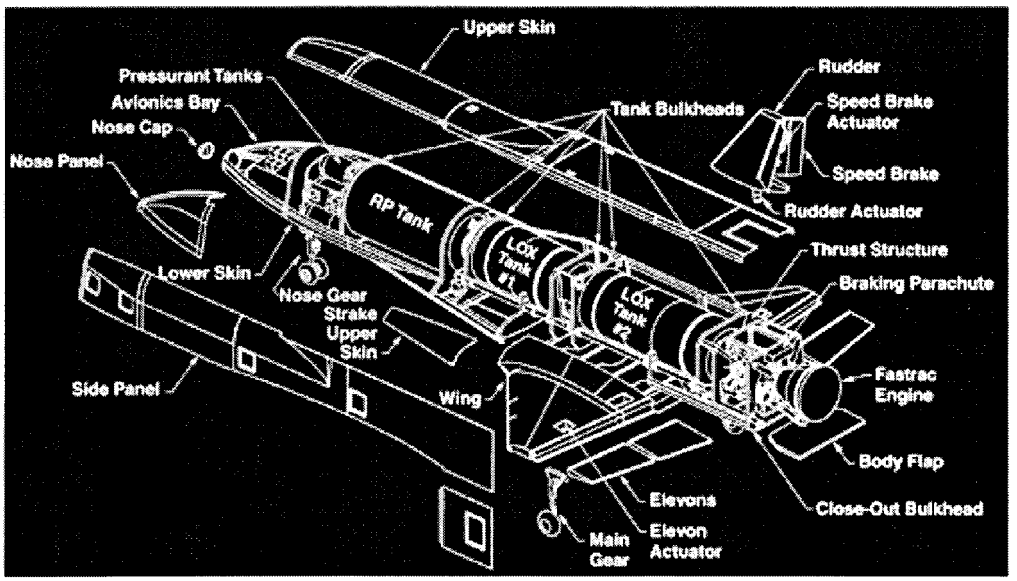

Fig. 3 X-34 design features.

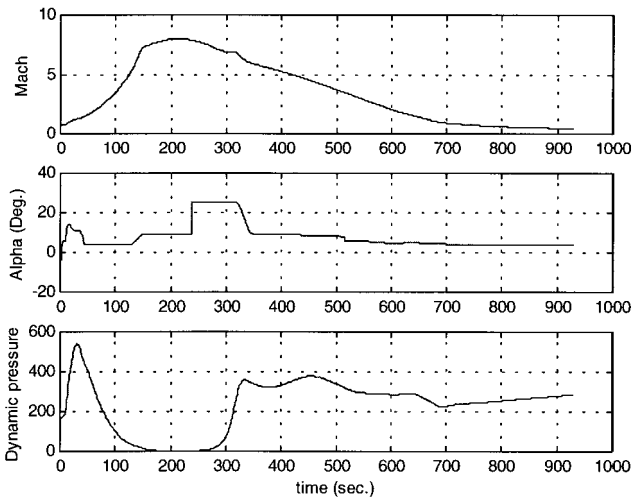

Fig. 4 Time history for maximum-Mach-number-mission (trajectory 3904).

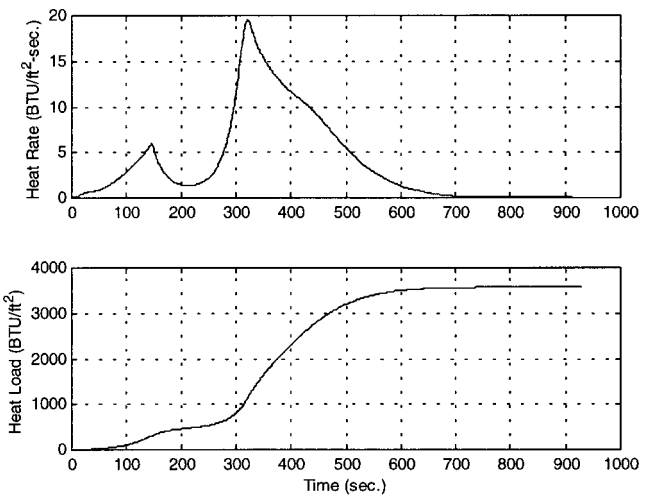

Fig. 5 Stagnation point heat rate and load for trajectory 3904.

of the heating predictions at less stressing conditions prior to the maximum-heating flights.

The typical maximum-Mach-number trajectory shown in Fig. 4 and referred to as trajectory 3904 begins after drop from the L-1011 carrier aircraft. The X-34 recovers from the separation, targets the engine fire attitude, and ignites the engine. The vehicle begins a pull-up maneuver as it quickly accelerates through maximum dynamic pressure ($t \sim 35$ s). Aerodynamic heating does occur on ascent, with stagnation heat rates of 6 BTU/ft^2-s being reached, but this is relatively benign when compared with re-entry heating. Dynamic pressure drops off rapidly as the vehicle enters the upper atmosphere, and when engine burnout is reached ($t \sim 145$ s) the vehicle is essentially exoatmospheric, with very little dynamic pressure. The X-34 then uses the reaction control system (RCS) to obtain a 25-deg angle of attack α for re-entry. As the vehicle begins to re-enter and decelerate, the maximum aerodynamic heating environment is reached, after which α is reduced to avoid skipping or bouncing on the atmosphere. Stagnation heat rates of 20 BTU/ft^2-s are reached. The vehicle then continues its autonomous descent through approach and landing.

Figure 5 shows the estimated stagnation point heat rate and load for this trajectory. The maximum temperature of the internal structure occurs 300–400 s after the maximum external heating event because it takes time for the heat to soak back into the structure.

Bounding Aerodynamic Heating Trajectories

A re-entry α of 25 deg means that the windward side and leading edges of the vehicle will see the highest temperatures and heat rates. The re-entry conditions are still severe as the vehicle transitions from 25- to 8-deg α, and at this point maximum leeward-side TPS temperatures and heat rates develop.

Given that the windward blanket temperatures cannot exceed the maximum HHB multiuse capability (2000°F), a balance must be struck between windward- and leeward-side maximum heating. If the vehicle were to attempt re-entry at an exceedingly high α, the temperatures at the lower-surface tile-to-blanket transition on the nose and wing leading edges could exceed the 2000°F limit. Likewise, if a re-entry or pull-out is attempted at a very low α, the leeward side of the nose and/or wing might reach maximum temperatures at the critical title-to-blanket transition location. Control issues such as minimizing altitude bounce and energy management require adherence to a certain α corridor.

Two bounding trajectories were developed to simulate maximum heating conditions for both the windward and leeward sides of the vehicle. These trajectories are referred to as 4701 and 4601, respectively. These bounding heating trajectories attempt to simulate high- and low-α re-entries but do not encompass 3 σ dispersions because margin was applied to the structural temperature limit.

Mach, α, q, and altitude profiles are presented in Figs. 6–9 for the three trajectories representing nominal (3904), maximum

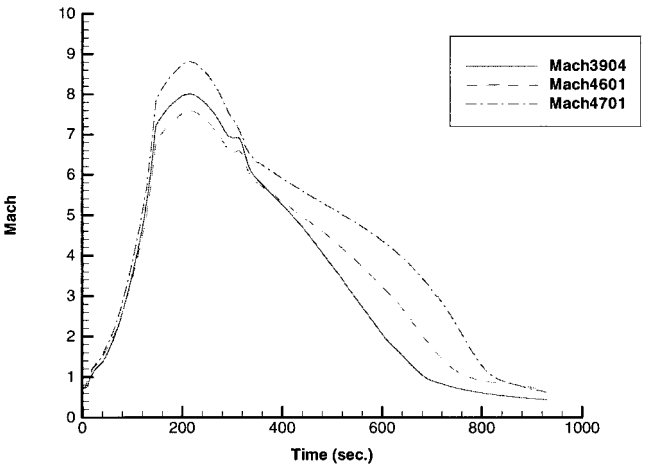

Fig. 6 Mach time history for 3904, 4601, and 4701 trajectories.

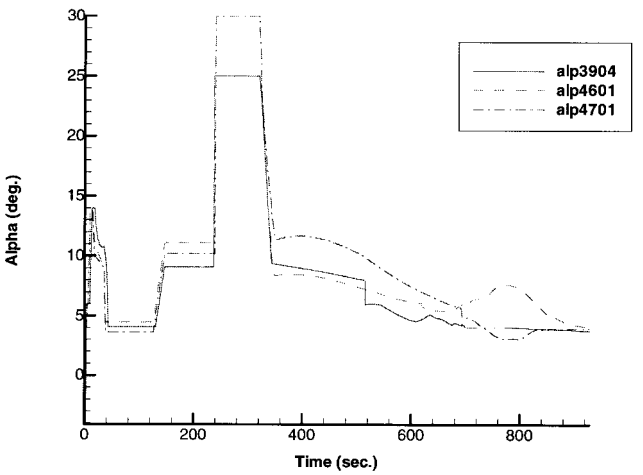

Fig. 7 α time history for 3904, 4601, and 4701 trajectories.

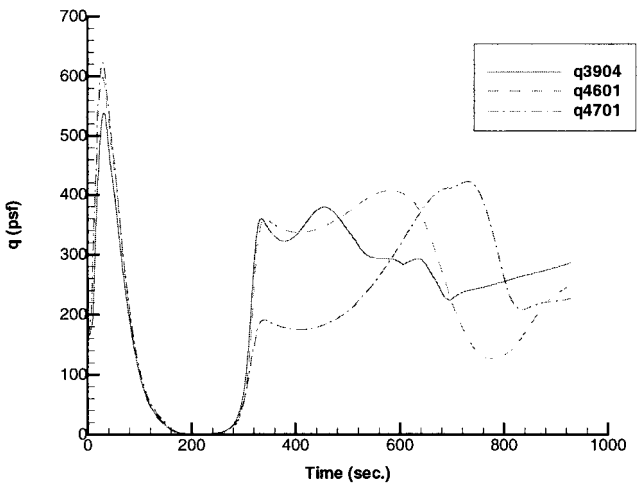

Fig. 8 Dynamic pressure time history for 3904, 4601, and 4701 trajectories.

windward-side heating (4701), and maximum leeward-side heating (4601).

Trajectory 4701 simulates a 30-deg α re-entry at much higher-than-intended energy. These conditions produce the maximum windward-side heating conditions. Most of the re-entry deceleration occurs at the high α prior to the transition to low α, and so this trajectory does not serve as a maximum for the leeward side of the vehicle.

Note that, at time 400 s, trajectory 4701 remains at a higher altitude and therefore lower air density than the other trajectories. The resultant dynamic pressure in this regime for trajectory 4701

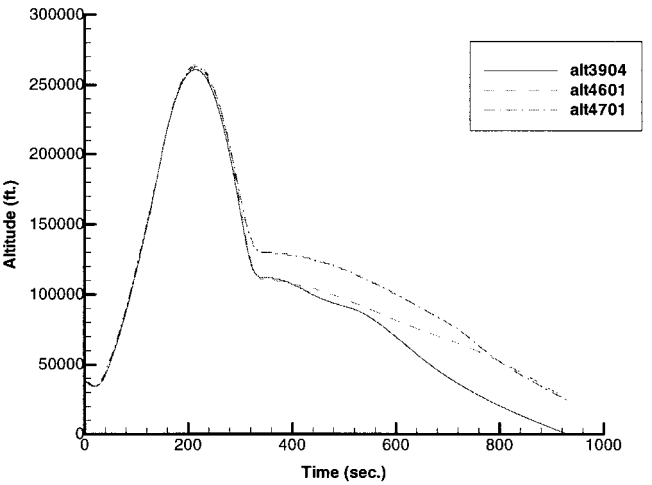

Fig. 9 Altitude time history for 3904, 4601, and 4701 trajectories.

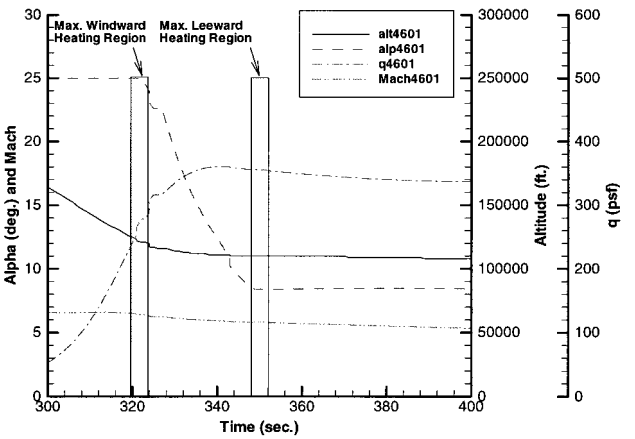

Fig. 10 Maximum windward- and leeward-side heating events for trajectory 4601.

is nearly half that of 4601. For this reason, 4601 was selected to simulate maximum leeward-side heating despite the fact that higher stagnation point heat rates are predicted for the other trajectories.

Trajectory 4701 holds a higher α throughout the re-entry pitch over 30–11 deg than both the 4601 and 3904 trajectories, whereas trajectory 4601 maintains a lower α (25–8 deg) than the current reference trajectory 3904 (25–10 deg). Overall these factors tend to drive trajectory 4601 to higher leeward-side temperatures and heat rates than both 4701 and 3904. Therefore, trajectory 4601 conditions were used by the NASA Langley Research Center aerothermal group for all detailed aerodynamic heating analyses and time histories, given that design flexibility was available only on the leeward side. Trajectory 4701 was used by the NASA Ames Research Center aerothermal group to analyze and test the leading-edge tiles and nose cap.

The critical conditions for maximum heating for the 4601 trajectory are highlighted in Fig. 10.

Aerodynamic Heating Analysis

The NASA Langley/Ames Research Center aerothermal group generated heating predictions using computational fluid dynamics (CFD) and experimental and analytical methods as presented in Refs. 6–12. In addition, data available from the Shuttle and X-15 were used for validation purposes.[13–19]

The analysis approach was to use CFD results for a given X-34 geometry (control deflections) and flight condition (Mach, altitude, α), along with experimental results to form an anchor for the aerothermal engineering code MINIVER.[20] This code was used to generate surface heating time history data at specific vehicle locations.

The computational methods predominantly used the LATCH[21] code in conjunction with inviscid flow solver results. The reduced

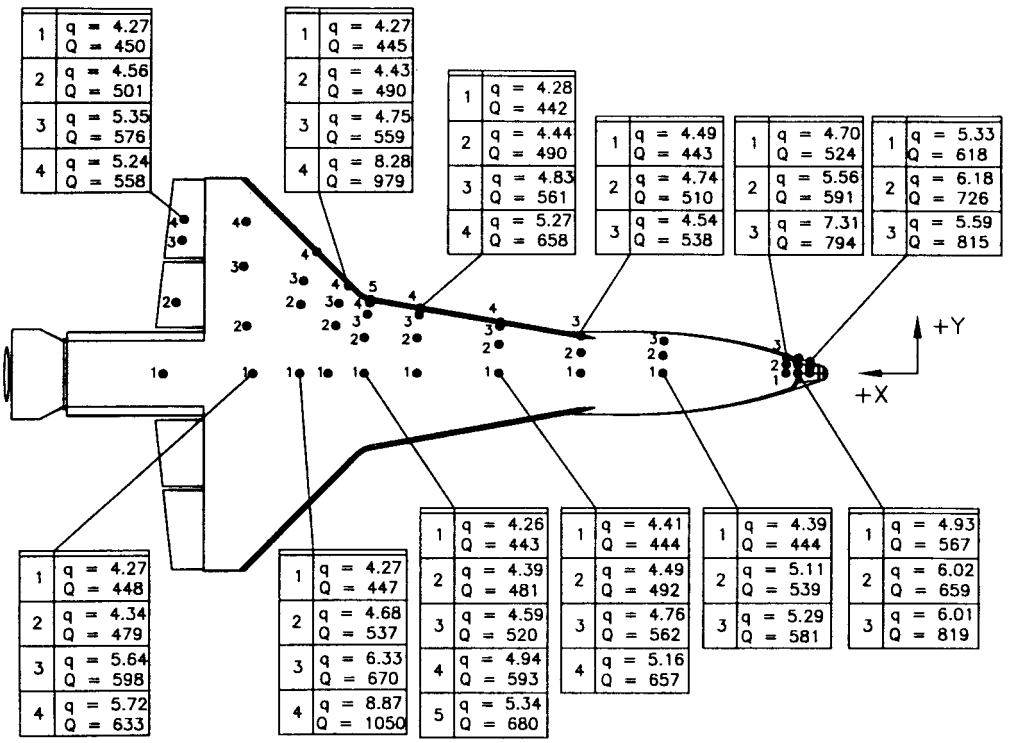

Fig. 11 Maximum windward-side heat rates and loads for trajectory 4601 (graphic courtesy of OTS): q = BTU/ft^2· s, and Q = BTU/ft^2.

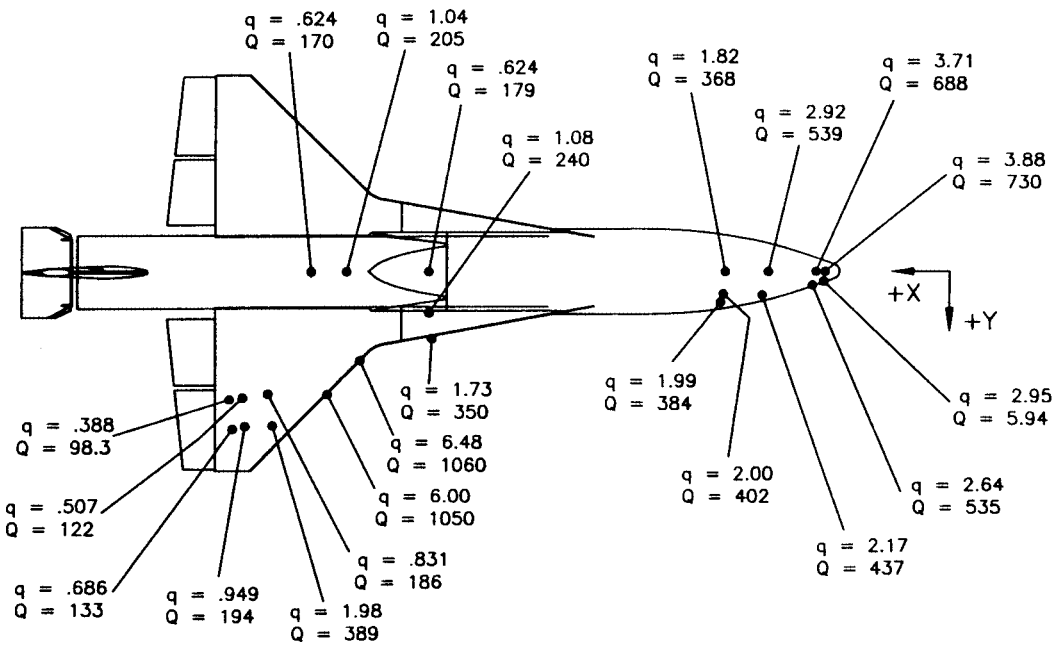

Fig. 12 Maximum leeward-side heat rates and loads for trajectory 4601 (graphic courtesy of OTS): q = BTU/ft^2· s and Q = BTU/ft^2.

grid generation and computational time associated with inviscid solutions enabled the team to run many more conditions than would have been possible with a viscous solver. The limited viscous solutions were used along with the tunnel results to check the Euler/LATCH method. This process proved very useful for the X-34 program by providing solutions at many conditions very quickly while only slightly sacrificing accuracy. The Euler/LATCH and viscous solutions were run at the points in the 4601 trajectory specified in Table 1.

The NASA Ames Research Center team used a similar approach with the 4701 trajectory to produce heating time histories for the nose cap and wing leading-edge tiles.

Flight Reynolds numbers will affect flow separation and shear on the vehicle. Because inviscid solutions do not account for separation, these methods were not used aft of the elevon trailing edges. Estimates for the aft body, body flap, and rudder were generated by scaling the heating time histories based on the limited viscous solutions that were obtained. Results from the heating tunnel were used to validate the assumptions made, especially in areas where flow separation is expected.

The following assumptions were used for analysis and uncertainty estimates:

1) Turbulent flow over all surfaces.

2) Shock impingement accounted for in uncertainty.

3) Trajectory dispersion (including atmospheric variations) accounted for in structural temperature margin.

4) Maximum re-entry elevon and body flap deflections of ± 10 deg.

5) Wall temperatures based on radiative equilibrium emissivity of 0.8.

Table 1 CFD analysis conditions

Time, s	Altitude, ft	Mach number	α, deg	Dynamic pressure, psf	Elevon, deg	Body flap, deg	Rudder, deg	Condition
145	182,995	6	9	21.9	0	0	0	Mach 6 ascent
152	196,437	6.83	11	16.4	0	0	0	Maximum heating ascent
330	118,419	6.32	23	299	0	0	0	Maximum windward heating
330	118,419	6.32	23	299	10	10	0	Maximum windward heating, +10-deg deflection
340	112,065	6	15.22	354	0	0	0	Match tunnel condition
355	110,314	5.8	8	356	−10	−10	0	Maximum leeward heating, −10-deg deflection
578	86,047	3.6	6.48	406	−10	−10	0	Maximum dynamic pressure during re-entry

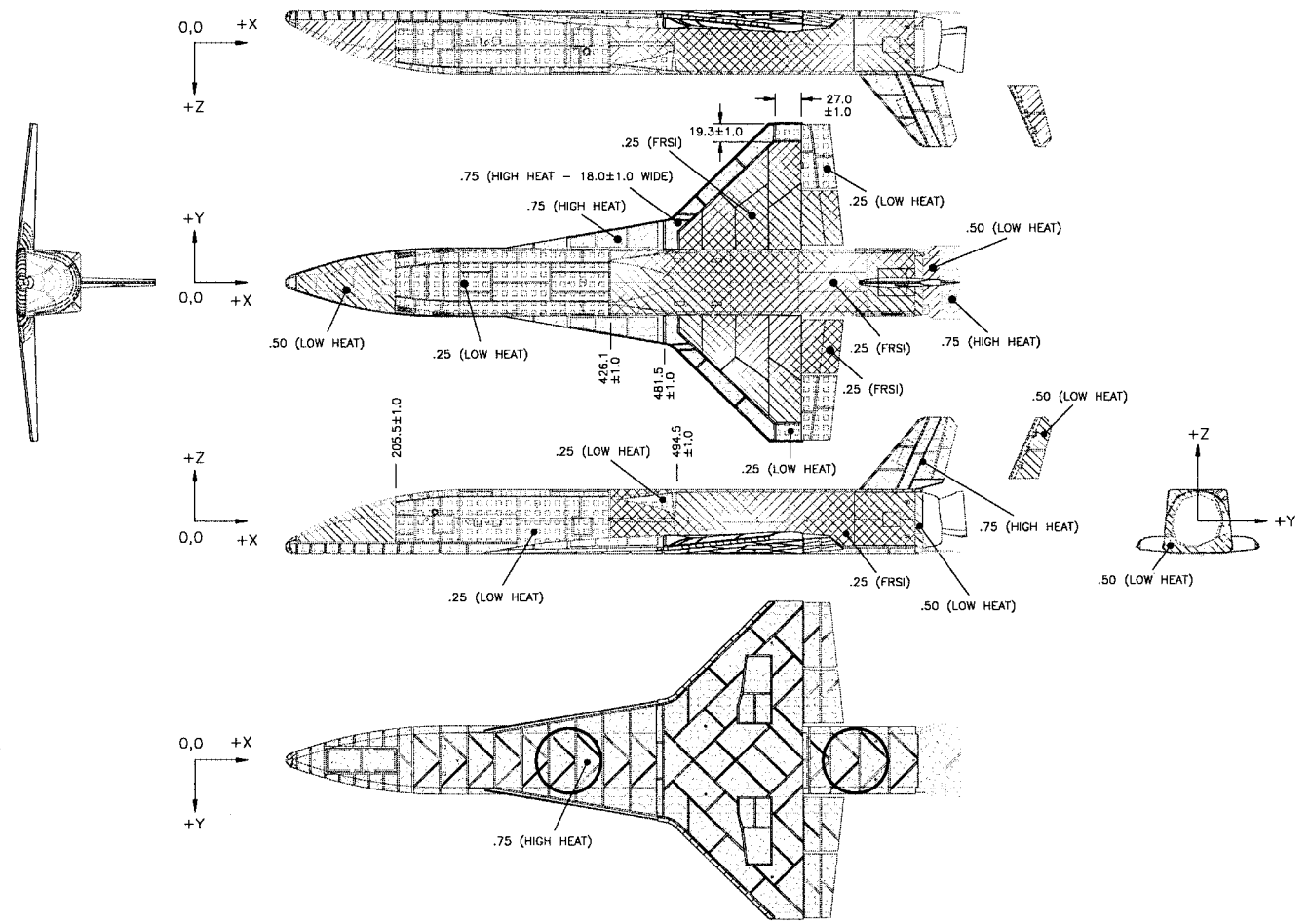

Fig. 13 Thermal protection blanket types and thickness distribution.

6) Perfect gas model for computational solutions.

7) Attached-flow, algebraic turbulence model in viscous solutions.

8) Attached-flow, integral boundary-layer turbulence model in LATCH.

9) Maximum windward-side heating conditions in the elevon and body flap gap area where simplifications were made for ease of grid generation.

10) Multiuse capability of the TPS blankets of HHB = 2000°F, LHB = 1500°F, and FRSI = 700°F.

Summary of Heating Results

All predicted temperatures are radiation equilibrium wall temperatures. The thermal mass of the structure is not taken into account until the complete thermal analysis is conducted with the proper heat transfer coefficients. Therefore, radiation equilibrium temperatures appear higher than expected adiabatic wall temperatures by 150–200°F.

Predicted windward-side radiation equilibrium temperatures are up to 2100°F on the nose tile, 2020°F on the wing leading-edge tile, 1800°F on the wing leading-edge blanket, and 1700°F on the elevon.

Maximum predicted leeward-side radiation equilibrium temperatures are 1300°F on the leeward nose blanket, 1800°F on the wing leading-edge blanket, and 900°F on the elevon.

A summary of maximum heat rates and loads at selected points on the vehicle is presented in Figs. 11 and 12. These points represent the areas for which complete heating time history data were generated. Estimates and interpolations were used for analysis in intermediate locations and on the side of the fuselage. Limitations in the Euler/LATCH method did not permit heating time histories to be developed aft of the elevon trailing edges. OSC estimated heating conditions for the aft fuselage, body flap, and rudder based on the limited viscous solutions that were generated. Again, a compromise was made between the timeliness and the completeness of the data to be generated.

TPS

Maximum predicted temperatures were used for the selection of the TPS type, and heat rate and load were used to select the TPS thickness required for insulation.

OTS is responsible for the design and manufacture of the TPS blankets. Figure 13 shows the blanket type and thickness selected for

Table 2 Summary of X-34 thermal protection materials

Material	Location	Multiple-flight temperature limit, °F	Multiple-flight heat flux limit, BTU/ft^2-s
SIRCA	Nose cap, wing leading edge, rudder leading edge	2600	175
HHB	Windward side, portion of leeward wing, rudder, speedbrake, and body flap	2000	20
LHB	Portions of fuselage and wing	1500	10
FRSI	Portions of fuselage and wing	700	2

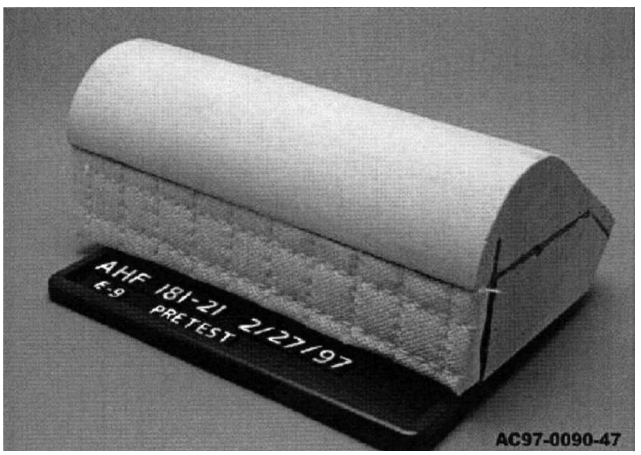

Fig. 14 SIRCA leading-edge tile and high-temperature AFRSI sample.

the X-34 based on the aerodynamic heating results. The circled areas on the windward side denote the locations for planned "piggyback" TPS experiments.

Table 2 provides a summary of the material capability and selection. Figure 14 shows a sample of the SIRCA tile and HHB on the wing leading edge. Note the stitch pattern evident on the blanket sample. The SIRCA tile builds up a black char layer after heating conditions are reached.

Local Heating Conditions

Some detailed heating analyses of the elevon hinge line and cove area were performed by the aerothermal group at NASA Ames Research Center. Similarly, heating analyses of the back side of the speed brake and body flap hinge line were performed by OSC. Sealing and protecting these areas has required some engineering judgment and novel approaches. In general, conservative assumptions were made in areas where data do not exist.

Aerodynamic heating conditions were used to size most of the X-34 TPS; however, the engine plume environment provides significant radiative and convective heating as well. The leeward side of the body flap and speed brake were analyzed based on engine plume heating predictions from MSFC, and the results showed that engine plume heating dominated. The TPS in these areas was sized specifically for the engine plume environment.

Conclusion

The X-34 program is attempting to push the edge of the envelope when it comes to the cost barrier to space access. To do this, NASA and OSC have had to balance technical risk, schedule, and cost in all areas. This was especially evident in the early design and analysis phase and in the area of aerodynamic heating. The aerothermal team at NASA Langley Research Center, NASA Ames Research Center, OTS, and OSC had to work under tight funding constraints within a seven-month window to produce the data used in the design of the X-34 TPS. To do this, the latest in CFD, experimental, and engineering methods were applied. The result is a design that is sufficiently optimized to meet the goals of the program.

References

[1] Sullivan, R. B., and Winters, B., "X-34 Program Overview," AIAA Paper 98-3516, July 1998.

[2] "X-34 to Be Acid Test for Space Commerce," *Aviation Week and Space Technology*, Vol. 142, No. 14, 1995, pp. 44–53.

[3] Brauckmann, G. J., "X-34 Vehicle Aerodynamic Characteristics," *Journal of Spacecraft and Rockets,* Vol. 36, No. 2, 1999, pp. 229–239.

[4] Sgarlata, P., and Winters, B., "X-34 Propulsion System Design," AIAA Paper 97-3304, July 1997.

[5] Dragone, T. L., and Hipp, P. A., "Materials Characterization and Joint Testing on the X-34 Reusable Launch Vehicle," 43rd International Society for the Advancement of Materials and Process Engineering Symposium, Covina, CA, June 1998.

[6] Wurster, K. E., Riley, C. J., and Zoby, E. V., "Engineering Aerothermal Analysis for X-34 Thermal Protection System Design," *Journal of Spacecraft and Rockets,* Vol. 36, No. 2, 1999, pp. 216–228.

[7] Kleb, W. L., Wood, W. A., Gnoffo, P. A., and Alter, S. J., "Computational Aeroheating Predictions for X-34," *Journal of Spacecraft and Rockets*, Vol. 36, No. 2, 1999, pp. 179–188.

[8] Palmer, G., and Polsky, S., "Heating Analysis of the Nosecap and Leading Edges of the X-34 Vehicle," *Journal of Spacecraft and Rockets*, Vol. 36, No. 2, 1999, pp. 199–205.

[9] Berry, S. A., Horvath, T. J., DiFulvio, M., Glass, C., and Merski, R. N., "X-34 Experimental Aeroheating at Mach 6 and 10," *Journal of Spacecraft and Rockets*, Vol. 36, No. 2, 1999, pp. 171–178.

[10] Merski, R. N., "Global Aeroheating Wind-Tunnel Measurements Using Improved Two-Color Phosphor Thermography Method," *Journal of Spacecraft and Rockets*, Vol. 36, No. 2, 1999, pp. 160–170.

[11] Riley, C. J., and Kleb, W. L., "Aeroheating Predictions for X-34 Using an Inviscid Boundary-Layer Method," *Journal of Spacecraft and Rockets*, Vol. 36, No. 2, 1999, pp. 206–215.

[12] Alter, S., "Surface Modeling and Grid Generation of Orbital Sciences X-34 Vehicle," NASA CR-97-206243, Nov. 1997.

[13] *Shuttle Performance: Lessons Learned*, NASA CP-2283, 1983.

[14] Throckmorton, D. A. (ed.), *Orbiter Experiments (OEX) Aerothermodynamics Symposium*, NASA CP-3248, 1995.

[15] Lliff, K. W., and Schafer, M. F., "A Comparison of Hypersonic Flight and Prediction Results," AIAA Paper 93-0311, Jan. 1993.

[16] Quinn, R. D., and Olinger, F. V., "Flight-Measured Heat Transfer and Skin Friction at a Mach Number of 5.25 and at Low Wall Temperatures," NASA TM-X-1921, Nov. 1969.

[17] Fricker, D., Mendoza, J., and Catton, I., "A Summary of the Computational Fluid Dynamics Analysis of the Hypersonic Flights of Pegasus," AIAA Paper 92-4059, Aug. 1992.

[18] Bertin, J. J., *Hypersonic Aerothermodynamics*, AIAA Education Series, AIAA, Washington, DC, 1994, pp. 90–149, 157–221.

[19] Jenkins, D. R., *Space Shuttle: The History of Developing the National Space Transportation System*, Walsworth, Marceline, MO, 1993, pp. 209–245.

[20] Engel, C. D., and Praharaj, S. C., "MINIVER Upgrade for the AVID System," Vol. 1: "LANMIN User's Manual," NASA CR-172212, Aug. 1983.

[21] Hamilton, H. H., Greene, F. A., and DeJarnette, F. R., "Approximate Method for Calculating Heating Rates on Three-Dimensional Vehicles," *Journal of Spacecraft and Rockets*, Vol. 31, No. 3, 1994, pp. 345–354.